VNU Journal of Science: Mathematics - Physics

Journal homepage: https://js.vnu.edu.vn/MaP

Original Article

Coma Aberration of a Nonlinear Aspherical Micro-Lens Created by Kerr medium

Pham Thanh Quang[1], Tran Quoc Tuan[1], Bui Xuan Kien[2,*]

Academy of Military Science and Technology, 17 Hoang Sam, Nghia Do, Hanoi, Vietnam

[2]Electric Power University, 235 Hoang Quoc Viet, Nghia Do, Hanoi, Vietnam

Received 15th January 2026
Revised 9th April 2026; Accepted 5th May 2026

Abstract: A nonlinear aspherical micro-lens (NAML) can be dynamically formed inside a Kerr medium under Gaussian beam (GB) illumination, providing an intensity-dependent optical surface that enables adaptive wavefront control. While previous studies have clarified the formation mechanism and spherical aberration of the NAML, the behavior of off-axis coma has not yet been fully investigated. In this work, we derive the complete third-order coma expression of the NAML by combining the nonlinear refractive-index distribution with the Seidel aberration formulation. The dependence of coma on the average laser power, nonlinear-layer thickness, and incident ray angle is examined through numerical simulations. The results show that the aspheric coma component dominates and scales strongly with $1/R^3$, leading to substantial wavefront distortion at large power, thickness, or field angle. A practical operating window is identified in which the coma remains within a few wavelengths. These findings establish the NAML as a power-tunable micro-optical element capable of partial off-axis aberration control.

Keywords: Nonlinear optics; Aspherical micro lens; Conic coefficient; Aberration optimization.

1. Introduction

Nonlinear optical media exhibiting an intensity-dependent refractive index provide a compact and powerful mechanism for self-induced wavefront shaping [1-3, 25, 33–36]. When a tightly focused GB propagates through a Kerr-type medium, the transverse variation of optical intensity gives rise to a refractive index modulation that behaves as an adaptive micro-lens. Such self-formed structures, commonly referred to as NAMLs, have attracted considerable interest due to their ultrafast response,

* Corresponding author.
E-mail address: kienpx@epu.edu.vn

https//doi.org/10.25073/2588-1124/vnumap.5111

simple fabrication-free formation, and compatibility with integrated and micro-optical systems [4-6]. Recent studies have demonstrated their potential in tunable focusing, adaptive beam steering, optical manipulation, and high-precision microscopy [7, 8, 11-13].

To analytically describe the behavior of these nonlinear lenses, a variety of models have been proposed, ranging from GRIN-type formulations to equivalent aspherical surface approximations [9-11, 15-17]. In particular, a recent study derived the curvature radius R and conic coefficient k of the NAML from the Kerr-induced index distribution and used them to evaluate the spherical aberration of the lens [12]. These works indicated that the spherical aberration can be effectively suppressed by tailoring the beam intensity, medium thickness, and nonlinear parameters of the material. Another related investigation on nonlinear GRIN lenses further highlighted the importance of including higher-order terms of the index distribution when predicting the aberration behavior of Kerr-induced micro-optics [13].

Despite these advances, the off-axis performance of the NAML remains insufficiently understood. In particular, third-order coma, one of the dominant off-axis aberrations in micro-optical systems, has not yet been quantitatively analyzed. Coma can severely distort the point-spread function by creating asymmetric tails and lateral shifts, thereby limiting the applicability of NAMLs in systems requiring precise off-axis imaging such as scanning microscopy, optical trapping, and miniaturized imaging modules [14, 15, 18-20]. Existing studies have focused predominantly on spherical aberration, leaving the coma characteristics of NAMLs unexplored.

To fill this gap, this paper presents the first comprehensive theoretical and numerical investigation of the coma aberration of a NAML formed inside a Kerr medium. By combining the Kerr-induced index modulation with the Seidel aberration theory, we derive the full expression of the third-order coma as a function of the average laser power, nonlinear layer thickness, and incident (field) angle. Numerical simulations reveal that the aspheric component of the coma-scaling strongly with $1/R^3$ - dominates under most operating conditions and increases significantly with power, film thickness, and field angle. Nevertheless, we identify a practical operating region in which the coma remains within a few wavelengths, enabling acceptable off-axis performance.

This work therefore extends previous analyses of nonlinear micro-lenses by providing a complete description of their off-axis aberration behavior. The results offer valuable guidelines for the design and optimization of power-tunable NAMLs in compact optical systems requiring both on-axis and off-axis wavefront quality.

2. Model of the Nonlinear Aspherical Micro-lens

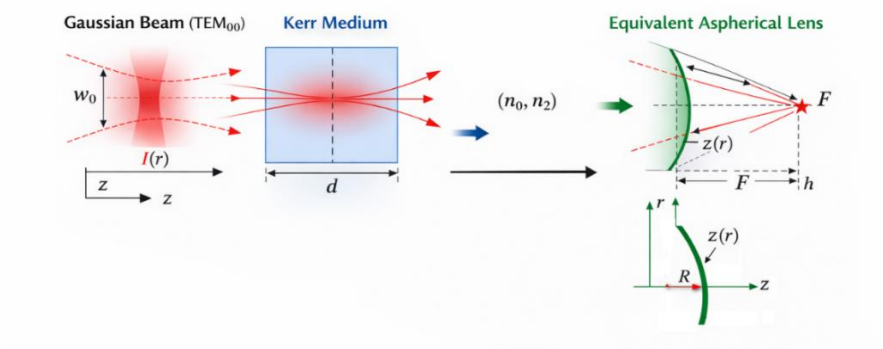

Figure 1. Model of a Kerr medium represented as an equivalent aspherical lens.

When a thin Kerr-type medium is illuminated by a tightly focused GB, the spatially varying optical intensity induces a corresponding modulation of the refractive index. This nonlinear modification produces an equivalent refracting profile whose geometry deviates from that of a classical spherical surface, giving rise to a NAML. Figure 1 illustrates the excitation configuration, the nonlinear index distribution, and the induced wavefront deformation. The analytical model describing the formation of this NAML is presented below.

In a Kerr medium, the refractive index depends on the local intensity through the relation [1, 2]:

$$n(r) = n_0 + n_2 I(r) \tag{1}$$

where n_0 is the linear refractive index, n_2 is the Kerr nonlinear coefficient, and $I(r)$ is the transverse intensity distribution.

For a TEM_{00} GB, the intensity profile at the beam waist is [3, 26]:

$$I(r) = I_0 \exp\left(-\frac{2r^2}{W_0^2}\right) \tag{2}$$

Because the lensing action is governed predominantly by the small ρ region, we expand the exponential term using a Maclaurin series and retain only the even orders relevant to symmetry:

$$n(r) = n_0 + n_2 I_0 \left(1 - \frac{2r^2}{W_0^2} + \frac{2r^4}{W_0^4}\right) \tag{3}$$

This radially varying index produces a spatially dependent optical path length. Under the thin-element approximation, the induced optical sag $z(\rho)$ which characterizes the deformation and is given by [9, 27-29]:

$$z(r) = \frac{2n_2 I_0 d r^2}{W_0^2} - \frac{2n_2 I_0 d r^4}{W_0^4} \tag{4}$$

Where d is the thickness of the nonlinear material.

These terms respectively represent the spherical and aspherical contributions to the induced surface profile. Compared with the typical GRIN-lens model which includes only the quadratic term, the appearance of a substantial quartic contribution demonstrates the inherently aspherical nature of the Kerr-induced nonlinear lens.

To identify the equivalent geometric parameters of the NAML, the sag above is compared to the standard aspheric-surface expression: By comparing the nonlinear sag above to the classical aspheric-surface representation,

$$z(r) = \frac{r^2}{R\left(1 + \sqrt{1 - (1+k) r^2 / R^2}\right)} \tag{5}$$

Using the Taylor expansion with the condition $r / R \to 0$, which is physically similar to the condition $0 < r << W_0$, the equation (5) will be:

$$z(\rho) = \frac{r^2}{R\left(1 + \sqrt{1 - (1+k) r^2 / R^2}\right)} = \frac{r^2}{2R} + \frac{r^4}{8R^3}(k+1) \tag{6}$$

Matching coefficients Eq. 4 and Eq. 6 leads to:

$$R = \frac{W_0^2}{4n_2 I_0 d_{phys}} \tag{7}$$

and

$$k = -1 - \frac{W_0^2}{4(n_2 I_0 d_{phys})^2} \tag{8}$$

Eq. 7 and Eq. 8 show that the equivalent aspherical surface is always hyperbolic *(k<-1)* and can be continuously tuned by varying the peak intensity or thickness of the Kerr layer.

These relations compactly express how the curvature and conic coefficient depend on the physical parameters of the nonlinear medium. In particular, both R and k vary with I_0, W_0, n_2, and d, meaning that the shape of the nonlinear lens can be modified continuously by adjusting the average power of the GB.

3. Coma Aberration

Coma is one of the most important third-order aberrations affecting off-axis image quality in high-resolution micro-optical systems. While spherical aberration describes the deviation of paraxial and marginal rays on the optical axis, coma arises when rays entering the lens with a small field angle experience asymmetric phase distortion, producing a characteristic comet-shaped blur in the focal region. For conventional aspherical lenses, coma is fixed by the manufactured surface profile; however, for a NAML, the optical surface is power-dependent and can therefore be dynamically tuned. This section establishes the analytical formulation of coma in the NAML and evaluates how it varies with the design parameters of the Kerr medium and the incident GB.

As demonstrated in Section 2, the nonlinear optical sag of the Kerr medium can be mapped to an equivalent aspherical surface characterized by the curvature radius R and conic coefficient k. For a thin aspherical refracting surface, the third-order coma aberration can be expressed using the Seidel formalism as the sum of the contributions from the spherical (base) component and the aspherical deviation: [30, 39-41]:

$$W_{131} = \frac{1}{2}\left(S_{II} + S_{IIa}\right) \tag{9}$$

where: S_{II} is the coma coefficient of the spherical component,

S_{IIa} is the coma coefficient induced by the aspheric deviation governed by the conic coefficient k.

The spherical-surface coma term is given by [1, 30-32]:

$$S_{II} = -n^2 yu\left(\frac{y}{R} + u\right)\left(\frac{\bar{y}}{R} + \bar{u}\right)\left(\frac{n}{n'^2} - \frac{1}{n}\right) \tag{10}$$

where:

- n: refractive index inside the Kerr layer;
- n': refractive index of the external medium (air);
- y: marginal-ray height;
- $\bar{y} = d\bar{u}$: chief-ray height at the nonlinear surface;
- u: marginal ray angle;

- $\bar{u}$: chief-ray angle;

S_{IIa} is determined by:

$$S_{IIa} = \frac{\bar{y}}{y} S_{Ia} = k\bar{y}\frac{y^3}{R^3}(n'-n) \tag{11}$$

Substituting Eqs. (10)–(11) into (9), the total third-order coma becomes:

$$W_{131} = -\frac{1}{2}n^2 yu\left(\frac{y}{R}+u\right)\left(\frac{\bar{y}}{R}+\bar{u}\right)\left(\frac{n}{n'^2}-\frac{1}{n}\right)+\frac{1}{2}k\bar{y}\frac{y^3}{R^3}(n'-n) \tag{12}$$

From Eq. 12, it is evident that the coma of the NAML is strongly governed by the curvature radius *R*, the conic coefficient *k*. Because both *R* and *k* are power-dependent quantities, the total coma can be actively tuned through the laser intensity, the nonlinear-layer thickness, and the field angle. In the next section, the dependence of the coma aberration on these parameters is numerically evaluated to demonstrate the feasibility of dynamically controlling the off-axis performance of the NAML.

4. Numerical Results and Discussion

To quantify the coma aberration of the NAML, we consider the same nonlinear medium and laser parameters as in the previous analysis of spherical aberration. In particular, the thin Kerr plate is modeled as a dry film of Oil Red O with linear refractive index $n_\rho = 1.45$, nonlinear coefficient $n_2 = 1.10^{-6} cm^2/W$, and physical thickness in the range $d = 0.6-1.5mm$ [7, 33-36]. The plate is placed at the beam waist of a Nd:YAG laser operating at $\lambda = 1.06\mu m$ in the TEM_{00} mode, generating a GB with waist radius $W_0 = 100\mu m$ [26, 37, 38]. For each average power P_{ave}, the corresponding peak intensity I_0, curvature radius R, and conic coefficient k are obtained from Eqs. (1)–(8), and then substituted into the coma expressions (9)–(15) to evaluate the total third-order coma W_{131} of the NAML.

4.1. Power-dependent Coma at Fixed Thickness

Fig. 2 shows the normalized coma W_{131}/λ as a function of the pupil coordinate r for different average powers P_{ave}, with the film thickness fixed at $d = 1.5mm$ and the marginal and chief ray angles set to $u = 2^0$, $\bar{u} = 2^0$ (in this study, we adopt the simplifying assumption $u = \bar{u}$; this choice does not limit generality, as the marginal and chief-ray angles are independent in the full Seidel formulation). For all powers, the coma vanishes at the pupil center and grows strongly toward the edges, exhibiting the typical odd symmetry of third order coma: negative on one side of the pupil and positive on the other. This behavior originates from the aspheric coma term, proportional to $k\bar{y}y^3/R^3(n'-n)$, which dominates over the spherical component for sufficiently large intensity.

As the average power increases from *1W* to *5W*, the magnitude of W_{131} grows rapidly. This trend is mainly driven by the reduction of the curvature radius $R \sim 1/n_2 I_0 d$, so that the factor $1/R^3$ in the aspheric coma term scales approximately as P_{ave}^3. Although the conic coefficient k gradually approaches -1 at higher powers, its variation is much weaker than the change in R, and therefore the

overall coma amplitude at the pupil edge can reach tens of wavelengths for the highest power considered. Compared to the spherical aberration analyzed in our previous work, where W_{040} stays within a few wavelengths under similar conditions, these results clearly indicate that power-induced coma can become the dominant limitation for off-axis performance of the NAML even when on-axis aberrations are well controlled.

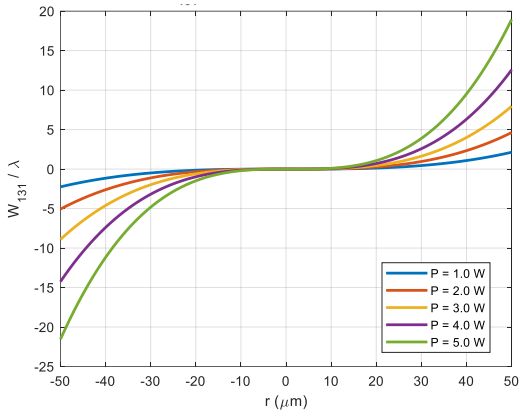

Figure 2. Coma W_{131} with different P_{ave} for d =1.5 mm, $u = \bar{u} = 2^0$.

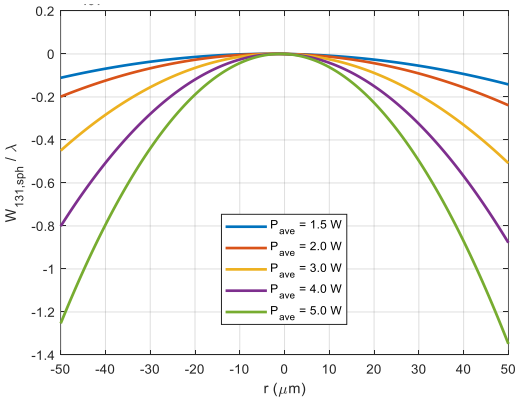

Figure 3. Coma W_{131} caused solely by the curvature radius R (with the conic term k omitted) for different P_{ave} at d=1.5mm, $u = \bar{u} = 2^0$.

Fig. 3 shows the normalized coma W_{131}/λ computed by retaining only the spherical-surface contribution associated with the curvature radius R, while omitting the aspheric term involving the conic coefficient k. In this case, the coma curves exhibit the characteristic odd symmetry of third-order Seidel coma, crossing zero at the pupil center and increasing toward the edges with opposite signs. The magnitude of the coma grows monotonically with the input power, which is consistent with the reduction of the nonlinear curvature radius R as the intensity increases. However, even at the highest power considered, the overall amplitude remains within only a few wavelengths, significantly smaller than the coma observed when the full aspheric contribution is included.

This behavior highlights the limited ability of curvature alone to generate large off-axis aberrations in the Kerr-induced lens. Because the spherical term depends primarily on the linear factors $(y/R+u)$ and $(\bar{y}/R+\bar{u})$, its contribution increases relatively slowly with power and does not lead to substantial distortion of the wavefront. The absence of the quartic dependence on y found in the aspheric term results in a much more moderate coma profile. This clearly indicates the potential for flexible coma correction when aspheric contributions are incorporated into optical system designs, as the dominant off-axis aberration can be effectively tailored through the conic term. These results confirm that the strong coma observed in the full model originates predominantly from the intensity-dependent asphericity (i.e., the k term), while the curvature-related component plays only a secondary role in defining the off-axis performance of the NAML. This finding highlights the potential for flexible aberration control, while emphasizing the need to carefully consider coma effects when aspheric components are incorporated into optical system designs.

4.2. Dependence on Nonlinear Layer Thickness

Fig. 4 illustrates the normalized coma W_{131}/λ as a function of the pupil coordinate r for several physical thicknesses of the nonlinear layer, ranging from $d = 0.6$ to 1.5mm, while keeping the average power fixed at $P_{ave} = 1W$ and the incidence angles at $u = \bar{u} = 2^0$. Similar to the previous case, all curves exhibit the characteristic odd symmetry of third-order coma. However, the magnitude of coma varies dramatically with the layer thickness.

When $d = 1.5mm$, the coma at the edge of the pupil reaches several tens of wavelengths, while for thinner layers (e.g., $d = 0.6mm$) the coma remains within a few wavelengths. These results indicate that reducing the physical thickness of the Kerr medium is an effective approach to suppressing coma, albeit at the cost of reduced nonlinear focusing strength. Therefore, the thickness of the nonlinear layer acts as a key design parameter that must be optimized to balance focal strength and off-axis image quality.

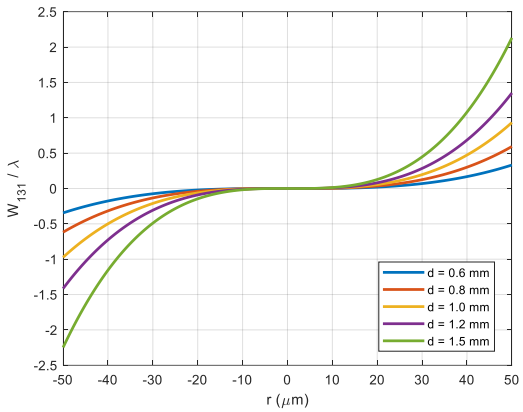

Figure 4. Coma W_{131} with different d for $P_{ave} = 1W$, $u = \bar{u} = 2^0$.

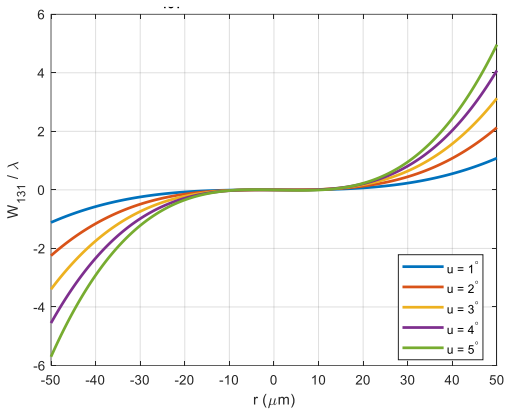

Figure 5. Coma W_{131} with different u for $P_{ave} = 1W$, $d = 1.5mm$.

4.3. Dependence on Marginal and Field Angle

Fig. 5 shows the normalized coma W_{131}/λ as a function of the pupil coordinate r for different marginal (field) angles, ranging from $u = \bar{u} = 1^0, 2^0, 4^0, 8^0$, with the physical thickness fixed at $d = 1.5mm$ and the average power set to $P_{ave} = 1W$. As expected, the coma maintains its odd-symmetric shape across the pupil, but its magnitude increases considerably as the field angle becomes larger.

For small angles such as $u = 1^0$, the coma amplitude remains within a few wavelengths, indicating that the NAML can still maintain acceptable off-axis performance. However, when the field angle reaches 4^0 or 8^0, the coma rises to several tens of wavelengths, dominated almost entirely by the aspheric term. In this regime, the focal spot becomes significantly distorted, making the NAML unsuitable for applications requiring a wide field of view or precise off-axis imaging.

Overall, the results clearly show that the field angle is a critical parameter governing coma in Kerr-induced NAMLs. Maintaining a small angular range is therefore essential for ensuring high-quality imaging or beam delivery, particularly when operating at high laser powers or with thick nonlinear layers.

5. Conclusion

We have developed a complete analytical and numerical framework for evaluating the coma aberration of a NAML formed in a Kerr medium. By deriving the full Seidel coma expression and incorporating the intensity-dependent curvature radius R and conic coefficient k, we demonstrated how the nonlinear refractive-index distribution directly shapes the off-axis wavefront of the NAML.

The numerical results show that the coma of the NAML depends strongly on the operating parameters. Variations in laser power, nonlinear-layer thickness, and field angle all lead to notable changes in the coma magnitude and its asymmetric distribution across the pupil. Under certain combinations of these parameters, the coma becomes large enough to significantly distort the focus; however, for moderate power levels, thin nonlinear layers, and small field angles, the coma remains within a manageable range.

Overall, the results confirm that the off-axis behavior of Kerr-induced micro-lenses is highly tunable and can be optimized through appropriate selection of system parameters. This establishes a solid foundation for designing adaptive nonlinear micro-optical elements with controllable coma performance for compact imaging and beam-shaping applications. These findings are consistent with previous studies on nonlinear lenses and aberration control [21–24, 30].

References

[1] B. E. A. Saleh and M. C. Teich, Fundamentals of Photonics, John Wiley & Sons, 2019.

[2] H. Q. Quy, V. N. Sau, N. T. T. Tam and N. V. Hoa, Nonlinear Coupler for Optical Fiber Mach–Zehnder Interferometers, Commun. Phys. 20, 2010, pp. 45–50

[3] R. Julius, A.–B. M. A. Ibrahim, P. K. Choudhury, A. N. Alias and M. S. Abd Halim, Quantum Features of The Nonlinear Coupler with Competing Nonlinearity, Sci. Rep. 12, 2022, pp. 8245.

[4] Q. Han, S. J. Elston, W. Kamal, L. Xue and S. M. Morris, A Nonlinear Model of Flexoelectric Liquid-Crystal Diffraction Gratings, Opt. Laser Technol. 180, 2025, pp. 111502.

[5] B. Wang and L. Pu, Design and Fabrication of Nonlinear Grating by Holographic Technology, CCIS 244, ICICA 2011, pp. 614–620.

[6] N. T. Q. Anh et al., Multiple Electromagnetically Induced Grating in The 85rb Five-Level Atomic Medium, J. Opt. Soc. Am. B 41, 2024, pp. 976–983.

[7] H. Q. Quy, M. V. Luu, T. D. Thanh, B. X. Kien, N. M. Thang, H. D. Quang, Optical Bistability of Partial Reflection–Coated Thin Film of Oil Red O, Appl. Opt. 59, 2020, pp. 5664–5669.

[8] Y.–P. Cai and R.–G. Wan, Bistable Reflection and Beam Shifts with Excitation of Surface Plasmons in a Saturable Absorbing Medium, Opt. Express 30, 2022, pp. 20725–20736.

[9] A. Kowalewska-Kudłaszyk, W. Leoński, T. D. Nguyen, V. C. Long, K. F. Renk, Kicked Nonlinear Quantum Scissors and Entanglement Generation, Phys. Scr. T160, 2014, pp. 014023.

[10] A. Kowalewska-Kudłaszyk and W. Leoński, Nonlinear Coupler Operating on Werner-Like States—Entanglement Creation Enhancement and Preservation, J. Opt. Soc. Am. B 31, 2014, pp. 1290–1297

[11] H. Q. Quy, T. T. Doan, T. Q. Tuan, N. M. Thang, Enhancement of Optical Trapping Efficiency by Nonlinear Optical Tweezers, Opt. Commun. 427, 2018, pp. 341–347.

[12] H. Q. Quy, T. T. Doan, T. Q. Tuan, N. M. Thang, Nonlinear Optical Tweezers for Longitudinal Control of Dielectric Particles, Opt. Commun. 421, 2018, pp. 94–98.

[13] H. Q. Quy et al., Nonlinear Microscope Objective Using a Thin Layer of Organic Dye for Optical Tweezers, Eur. Phys. J. D 74, 2020, pp. 52.

[14] B. X. Kien, D. V. Chau and H. Q. Quy, Aspherical Behaviors of The Kerr Medium Irradiated by a Gaussian Beam, J. Nonlinear Opt. Phys. Mater. Vol. 35, No. 01, 2026, pp. 2550004

[15] D. T. Moore, Gradient-Index Optics: A Review, Appl. Opt. 19, 1980, pp. 1035–1038.

[16] A. Hasnaoui, M. Fromager and K. Ait-Ameur, On the Validity of the Parabolic Approximation in Kerr Lensing Effect, Optik 193, 2019, pp. 162986.

[17] S. Leghmize et al., On The Different Ways for Defining the Effective Focal Length of a Kerr Lens, Laser Phys. 27, 2017, pp. 106201.

[18] A. Sattin et al., Aberration Correction in Long Grin Lens–Based Microendoscopes for Extended Field-of-View Two-Photon Imaging, eLife, 2024.

[19] W. M. Lee and S. H. Yun, Adaptive Aberration Correction of Grin Lenses for Confocal Endomicroscopy, Opt. Lett. 36, 2011, pp. 4608–4610.

[20] F. Bortoletto et al., Multiphoton Fluorescence Microscopy with Grin Objective Aberration Correction by Low-Order Adaptive Optics, PLoS ONE 6, 2011.

[21] R. G. González-Acuña and H. A. Chaparro-Romo, General Formula for Bi-Aspheric Singlet Lens Design Free of Spherical Aberration, Appl. Opt. 57, 2018, pp. 9341–9345.

[22] H. Qin, Aberration Correction of a Single Aspheric Lens with Particle Swarm Algorithm, Opt. Commun. 285, 2012, pp. 2996–3000.

[23] A. Miks and P. Pokorný, Spherical Aberration of an Optical System and Its Influence on Depth of Focus, Appl. Opt. 56, 2017, pp. 5099–5107.

[24] S. Vazquez-Montiel and O. García-Lievanos, Spherical Aberration Correction Using Aspheric Surfaces, Rev. Mex. Fis. 59, 2013, pp. 273–281.

[25] A. Hasnaoui et al., Structuring a Laser Beam Subject to Optical Kerr Effect for Improving Its Focusing Properties, Appl. Phys. B, Vol 127(5), 2021, pp.75.

[26] K. F. Renk, Basics of Laser Physics, Springer, 2017.

[27] A. D. Polyanin and A. V. Manzhirov, Handbook of Mathematics for Engineers and Scientists, CRC Press, 2016.

[28] R. Schuhmann, Description of Aspheric Surface, Adv. Opt. Technol. 8, 2019, pp. 267–278.

[29] J. Sasian, Introduction to Lens Design, Cambridge Univ. Press, 2019.

[30] J. A. Strother, Reduction of Spherical and Chromatic Aberration in Axial-Scanning Optical Systems with Tunable Lenses, Biomed. Opt. Express 12, 2021, pp. 3530–3552.

[31] G. Forbes, Shape Specification for Axially Symmetric Optical Surfaces, Opt. Express 15, 2007, pp. 5218–5226.

[32] R. R. Krishnamurthy and R. Alkondan, Nonlinear Characterization of Mercurochrome Dye for Optical Limiting, Opt. Appl. 40, 2010, pp. 187–196.

[33] H. A. Badran et al., Laser-Induced Optical Nonlinearities in Orange G Dye: Polyacrylamide Gel, Can. J. Phys. 89, 2011, pp. 1219–1224.

[34] S. Jeyaram and T. Geethakrishnan, Third-Order Nonlinear Optical Properties of Acid Green 25 Dye by Z-Scan Method, Opt. Laser Technol. 89, 2017, pp. 2570–2574.

[35] L. T. Nguyen et al., Numerical Methods for Analyzing Z-Scan Data, J. Nonlinear Opt. Phys. Mater. 23, 2014, pp. 1450020.

[36] K. Lee et al., Non-Resonant Power-Efficient Directional Nd:Yag Ceramic Laser Using a Scattering Cavity, Nat. Commun. 12, 2021, pp. 8.

[37] K. M. Abedin et al., Power Stability of Different Lasers and Its Effect on Phase-Stepping Shearography, Results Opt. 12, 2023, pp. 100490.

[38] P. D. Quy et al., Calculation and Design of Thermal Object Lens Using an Aspherical Lens for Handheld Observation Devices, J. Military Sci. Technol. 76, 2022, pp. 127–136.

[39] S. Sparrold and A. Lansing, Spherical Aberration Compensation Plates, Opt. Comp. Photonic Int., 2011.

[40] D. C. Compertore et al., Development of a Calibration Standard for Spherical Aberration, Proc. SPIE, 2013.

[41] D. Malacara, Handbook of Lens Design, Marcel Dekker, 1994.